Supplementary Information

One-pot Fabrication of Novel Urchin-like Fe_3O_4/α-FeOOH/$Al(OH)_3$ Magnetic Nanocomposite for Phosphate Removal and Recovery: Adsorption Performance and Mechanism

Yu-Han Wang[1,2], Wei Yin[1,2], Wen-Ping Liu[1,2], Qi-Zhi Yao[3], Sheng-Quan Fu[4], Gen-Tao Zhou[1,2*]

[1] Deep Space Exploration Laboratory/School of Earth and Space Sciences, University of Science and Technology of China, Hefei 230026, China

[2] State Key Laboratory of Lithospheric and Environmental Coevolution, University of Science and Technology of China, Hefei 230026, China

[3] School of Chemistry and Materials Science, University of Science and Technology of China, Hefei 230026, China

[4] Hefei National Laboratory for Physical Sciences at the Microscale, University of Science and Technology of China, Hefei 230026, China

Corresponding author: Prof. Dr. Gen-Tao Zhou

Tel.: 86 551 63600533

Fax: 86 551 63600533

Email: gtzhou@ustc.edu.cn

Table S1. The determined content of $Al(OH)_3$ in MGA nanocomposite.

Sorbents	Content of $Al(OH)_3$ (%)
MGA10	7.6 ± 0.4[a]
MGA20	13.2 ± 0.8
MGA30	19.6 ± 1.1
MGA40	24.5 ± 1.3
MGA50	26.2 ± 2.3

[a] Average ± standard deviation (n=3).

Text S1 Influence of synthesis parameters and reaction pathway on MG formation.

The successful co-synthesis of magnetite and goethite (MG) during the oxidation of aqueous Fe(II) suspensions is highly sensitive to reaction parameters, particularly temperature and stirring speed [1]. Fig. S1 depicts the XRD patterns of the oxidation products obtained at varying temperatures (40 and 60 °C) and stirring speeds (200 and 400 rpm). The results demonstrate that the desired biphasic composition of Fe_3O_4 and α-FeOOH is exclusively achieved at 60 °C with a stirring speed of 200 rpm (Fig. S1a). When the temperature is maintained at 60 °C but the stirring speed is increased to 400 rpm, the resulting precipitate consists of goethite and lepidocrocite (γ-FeOOH) (Fig. S1b). This phase shift is likely attributable to the enhanced air/suspension interfacial interactions at higher stirring speeds, which accelerates oxygen dissolution and kinetically favors lepidocrocite formation [1]. Furthermore, when the stirring speed is kept at 200 rpm but the temperature is lowered to 40 °C, magnetite is absent from the final product (Fig. S1c). This variation underscores the critical role of temperature in modulating oxygen solubility; typically, elevated temperatures (≥ 60 °C) reduce oxygen solubility and preferentially drive the formation of Fe_3O_4, whereas lower temperatures with higher oxygen solubility favor lepidocrocite [1]. This preferential formation of magnetite at higher temperatures aligns with the observations by Wang et al. and Kiyama at 75 °C and 80 °C, respectively [2,3].

Beyond temperature and aeration, the crystallization pathway of magnetite is strictly governed by the initial reactant ratio ($[Fe^{2+}]/[OH^-]$). Based on particle shape evolution, Kiyama [2] concluded two distinct formation mechanisms: under highly alkaline conditions ($[Fe^{2+}]/[OH^-] < 0.5$), octahedral or cubic magnetite precipitates directly from $Fe(OH)_2$; conversely, when OH^- is insufficient ($[Fe^{2+}]/[OH^-] > 0.5$), the reaction proceeds via a hexagonal green rust intermediate, ultimately transforming into spherical magnetite. In our synthesis, the initial $[Fe^{2+}]/ [CH_3COONa]$ ratio was set to 0.5. Because CH_3COO^- ions undergo slow hydrolysis to gradually release OH^- [4], the real-time $[Fe^{2+}]/[OH^-]$ ratio consistently remains greater than 0.5. This kinetically controlled release of hydroxyl ions effectively suppresses the direct precipitation of $Fe(OH)_2$, forcing the oxidation to proceed via the green rust pathway. Consequently, the observation of spherical magnetite nanoparticles in our HRTEM results (Fig.

2b) corroborates this mechanistic deduction, confirming that the magnetite in the MG composite evolved via the transformation of green rust intermediates.

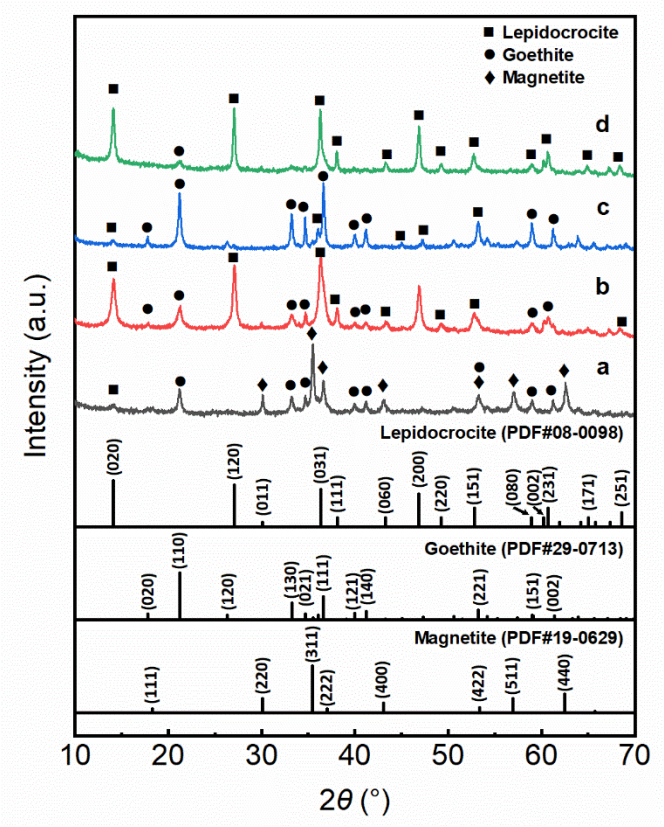

Fig. S1 XRD patterns of products obtained from oxidation of $Fe(OH)_2$ at the temperature of 60 °C and stirring speed of 200 (a) and 400 (b) rpm, and at the temperature of 40 °C and stirring speed of 200 (c) and 400 (d) rpm.

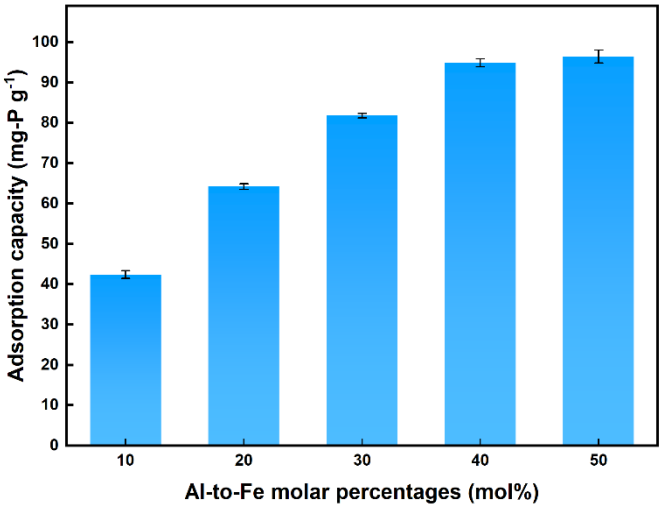

Fig. S2 Effect of Al-to-Fe molar percentages on the phosphate adsorption capacity of MGA nanocomposites.

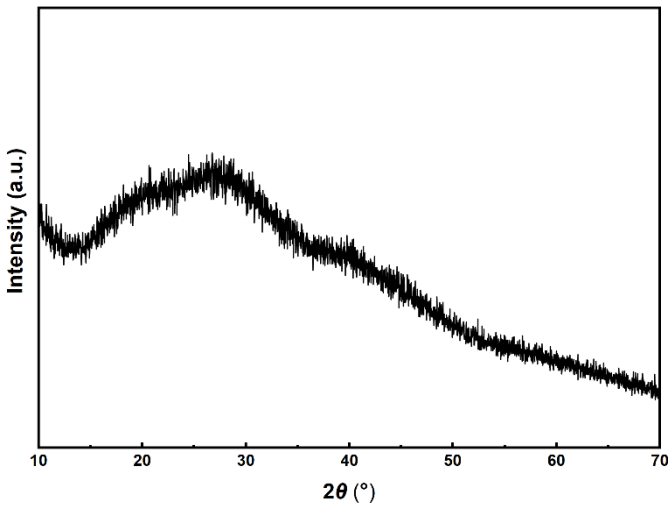

Fig. S3 XRD pattern of the aluminum precipitate obtained at the temperature of 60 °C and stirring speed of 200 rpm without the MG substrate

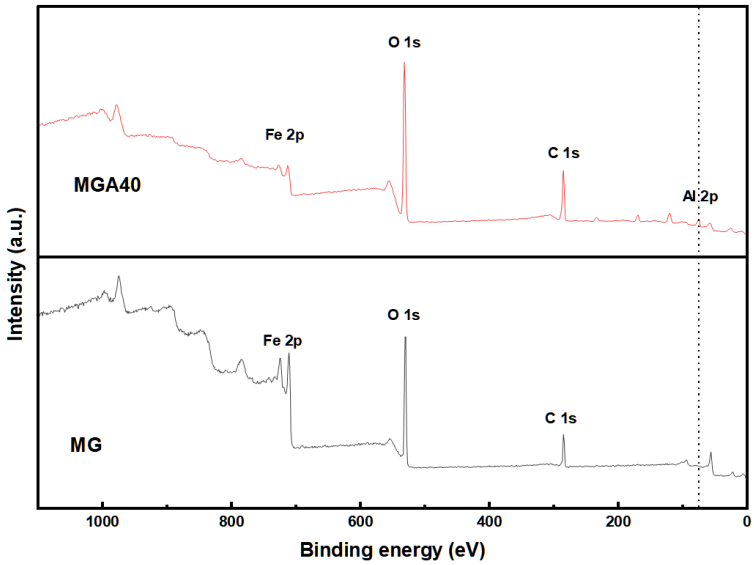

Fig. S4 XPS survey of the MG and MGA40 nanocomposites.

Table. S2 Pore Structure Characterization of MG and MGA.

Sample	S_{BET} (m^2/g)	Average pore diameter (nm)
MG	39.79	14.77
MGA	77.98	7.64

Table S3. Fitted parameters for the pseudo-first-order kinetics and Langmuir isotherm of phosphate adsorption on MGA.

Sorbents	Pseudo-first-order kinetics			Langmuir isotherm		
	k_1 (min^{-1})	Predicted q_e (mg-P/g)	R^2	q_{max} (mg-P/g)	K_L (L/mg)	R^2
MGA10	0.0287	37.12	0.9140	40.78	4.96	0.8336
MGA20	0.0306	55.79	0.9162	53.19	135.58	0.6199
MGA30	0.0329	65.68	0.9240	73.23	61.45	0.8324
MGA40	0.0340	76.95	0.9298	86.69	66.21	0.8883
MGA50	0.0331	77.89	0.9297	84.31	68.50	0.8284

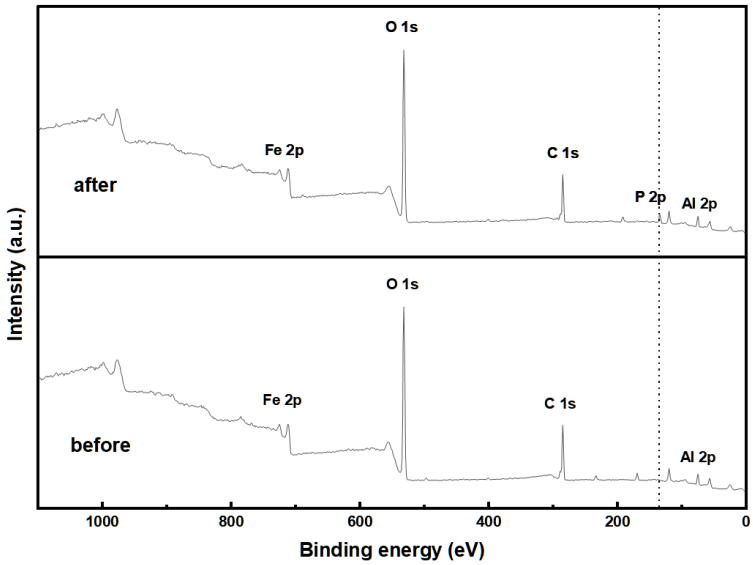

Fig. S5 XPS survey of the MGA40 before and after phosphate adsorption.

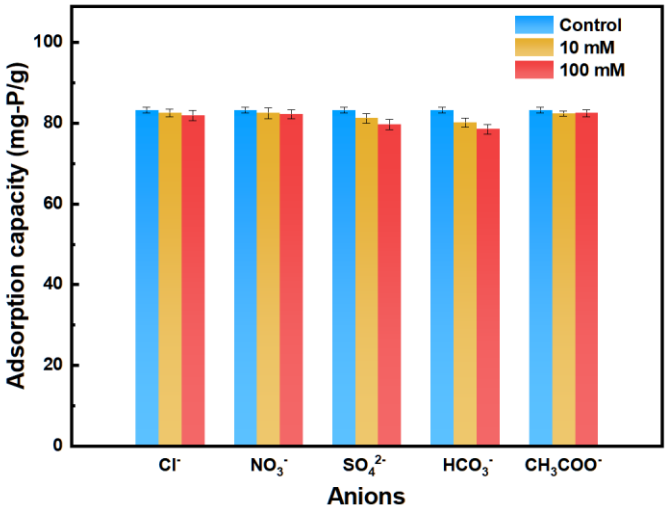

Fig. S6 Effects of co-existing anions on phosphate adsorption of MGA nanocomposites.

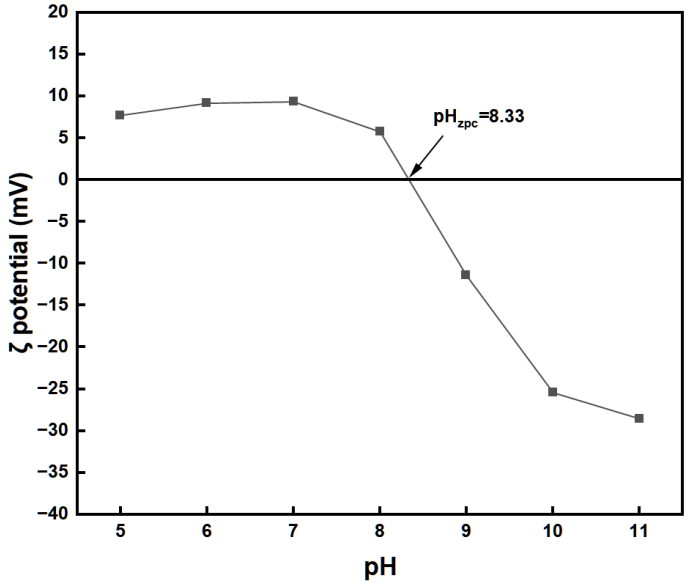

Fig. S7 ζ potential of the MGA40 nanocomposite.

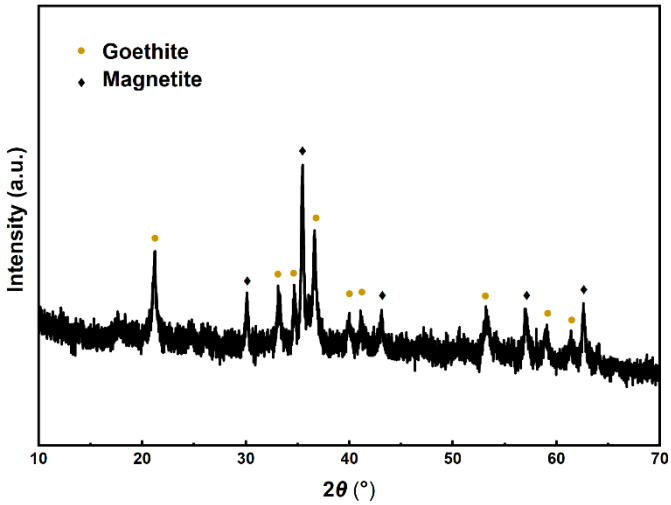

Fig. S8 XRD pattern of the MGA40 after five adsorption-desorption cycles.

References

[1] F. Gilbert, P. Refait, F. Lévêque, C. Remazeilles, E. Conforto, Synthesis of goethite from Fe(OH)2 precipitates: Influence of Fe(II) concentration and stirring speed, J. Phys. Chem. Solids 69 (2008) 2124–2130. https://doi.org/10.1016/j.jpcs.2008.03.010.

[2] M. Kiyama, Conditions for the formation of Fe 3 O 4 by the air oxidation of Fe (OH) 2 suspensions., Bull. Chem. Soc. Jpn. 47 (1974) 1646–1650.

[3] G. Wang, M.E. Bowden, S.A. Saslow, B.J. Riley, D.-S. Kim, W.C. Eaton, A.A. Kruger, Micrometer-sized magnetite synthesis using Fe(OH)2(s) as a precursor for technetium sequestration from liquid nuclear waste streams, J. Nucl. Mater. 552 (2021) 152964. https://doi.org/10.1016/j.jnucmat.2021.152964.

[4] Q. Hao, S. Liu, X. Yin, Y. Wang, Q. Li, T. Wang, Facile synthesis of 3D flowerlike α-FeOOH architectures and their conversion into mesoporous α-Fe2O3 for gas-sensing application, Solid State Sci. 12 (2010) 2125–2129. https://doi.org/10.1016/j.solidstatesciences.2010.09.010.